# Viral tracing identifies distributed columnar organization in the olfactory bulb

David C. Willhite*†, Katherine T. Nguyen*, Arjun V. Masurkar*, Charles A. Greer*‡, Gordon M. Shepherd*, and Wei R. Chen*

Departments of *Neurobiology and ‡Neurosurgery, Yale University School of Medicine, 333 Cedar Street, New Haven, CT 06510

Edited by Dale Purves, Duke University Medical Center, Durham, NC, and approved June 26, 2006 (received for review March 17, 2006)

**Olfactory sensory neurons converge onto glomeruli in the olfactory bulb (OB) to form modular information processing units. Similar input modules are organized in translaminar columns for other sensory modalities. It has been less clear in the OB whether the initial modular organization relates to a columnar structure in the deeper layers involved in local circuit processing. To probe synaptic connectivity in the OB, we injected a retrograde-specific strain of the pseudorabies virus into the rat OB and piriform cortex. The viral-staining patterns revealed a striking columnar organization that extended across all layers of the OB from the glomeruli to the deep granule cell layer. We hypothesize that the columns represent an extension of the glomerular unit. Specific patterning was observed, suggesting selective, rather than distance-dependent, center-surround connectivity. The results provide a previously undescribed basis for interpreting the synaptic connections between mitral and granule cells within the context of a columnar organization in the OB and have implications for olfactory coding and network organization.**

columns | olfaction | pseudorabies virus | synaptic tracing

The mammalian brain receives a diverse array of information about the external environment through highly varied sensory modalities. In sensory systems as dissimilar as somatosensation, vision, and audition, a common organizing principle has emerged within the sensory cortices, the cortical column. Lorente de Nó (1) first suggested a higher-order columnar organization of neurons based on Golgi impregnation anatomy of cortical cells. Electrophysiological evidence in the somatosensory cortex later showed that neurons responded to deep or superficial mechanical stimulation in grouped, vertical columns (2). This organizational principle was subsequently found in other sensory areas such as visual (3, 4) and auditory cortices (5) and in higher-order areas such as association cortex (6). The olfactory bulb (OB) is a cortical region for which there have been indications of possible columnar connectivity, but this organizational principle has not been explored as thoroughly in the OB as in other brain regions.

In the olfactory system, the segregation of sensory information begins with the convergence of olfactory sensory neuron (OSN) axonal subpopulations onto specific glomeruli (Fig. 6, which is published as supporting information on the PNAS web site) (7). In rodents, the axons of 10,000 OSNs expressing the same olfactory receptor type in the nasal epithelium converge onto at least two glomeruli in each OB, one lateral and one medial, arising from OSNs in the medial and lateral epithelium, respectively (8–13). The glomerulus and the intrabulbar neurons synaptically connected within it are thought to represent a modular information processing unit that sends odor information to pyramidal neurons in the olfactory cortex and other brain areas via the projection neurons, mitral and tufted cells.

Olfactory projection neurons receive inhibition at the glomerular level by periglomerular cells (14) and by granule cells that form synapses on the soma and lateral dendrites of mitral and tufted cells (15–18). The lateral dendrites of mitral and tufted cells can extend >1,000 microns and are thought to play a key role in OB lateral inhibition through their granule cell connections (19–22). This inhibitory network is modulated further by centrifugal fibers from the olfactory cortex and other distal brain regions (23, 24). Processing thus proceeds through two main levels, glomerular and granular, but the relationships between the two are not understood.

To probe this relationship, we used a tracer, the pseudorabies virus (PRV), which has been used as a marker of synaptic connectivity in other systems. PRV is neuron specific and passes transsynaptically to infect new neurons and renew the replication cycle (25). The Bartha strain used in this work is retrograde-specific, and expresses the GFP or mRed1 for visualization (PRV-152 or PRV-614, respectively) (26–30).

Using this approach, we found a radial synaptic connectivity pattern in the OB extending from the glomeruli to the deep granule cell layer, which further analysis showed to be columnar. The observed labeling suggests inhibition patterns arising from granule cells activated by mitral and tufted cell secondary dendrites that are distributed among specific clusters of granule cells, rather than continuously graded inhibition as a function of distance.

## Results

**Pseudorabies Infection Cycle in the Olfactory System.** To probe OB circuit organization, we made local PRV injections into the OB. In a representative experiment, the injection site diameter was ≈300 $\mu$m, covering 4–8 glomeruli (Fig. 1). After 1 day of infection, fluorescence at the infection site is faint and only found in cells whose cell bodies are proximal to the injection site. After 2 days of infection, cell labeling was clearly visible by GFP fluorescence and revealed that mitral/tufted cells in the injected glomerulus were infected and passed virus into the granule cell layer (GCL) locally (Fig. 7, which is published as supporting information on the PNAS web site). Three days after infection, virus had extended to specific neuron populations through most of the OB.

It was evident from inspecting the labeling in the immediate area of the injection site that the cell populations were not labeled randomly but in restricted patterns. Of most interest was the pattern of granule cell labeling that, in Fig. 1, can be seen to consist of several groups of cells oriented perpendicular to the plane of the mitral cell layer. We extended our observations throughout the OB to determine the degree of lateral virus spread. To establish that the pattern was not a region-specific effect, we made injections into different parts of the OB (Fig. 7*A*).

Conflict of interest statement: No conflicts declared.

This paper was submitted directly (Track II) to the PNAS office.

Abbreviations: GCL, granule cell layer; LOT, lateral olfactory tract; OB, olfactory bulb; PRV, pseudorabies virus; SVZ, subventricular zone.

†To whom correspondence should be addressed. E-mail: david.willhite@yale.edu.

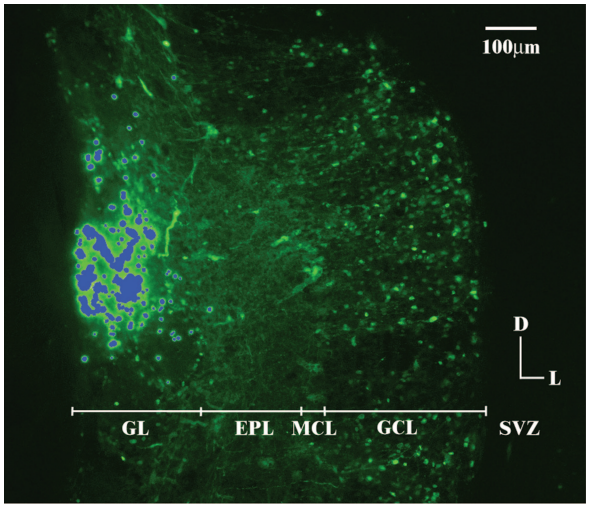


**Fig. 1.** An OB injection site. Coronal section of the rat brain 3 days after PRV injection into the anterior dorsomedial OB viewed at ×100 magnification. Virus-infected cells are visible in green (GFP), green fluorescent beads were included as a marker of the injection site, and they are easily distinguished from viral staining in practice by intensity and punctate appearance. Beads are false colored blue for clarity. GL, glomerular layer; EPL, external plexiform layer; MCL, mitral cell layer; SVZ, subventricular zone. Orientation bar indicates dorsal and lateral.

**Retrograde Tracing in the OB Reveals Radial Patterning.** A representative result of an experiment to test for synaptic connectivity patterns throughout the OB for PRV injected into the anterior dorsolateral OB (see *Materials and Methods*) is shown in Fig. 2 *A–C*. Pyramidal cells in much of the anterior piriform cortex (PC) were brightly labeled (Fig. 2*A*). The lateral olfactory tract (LOT) was only lightly labeled, consistent with the observation of relatively few labeled mitral and tufted cell bodies in the OB. A few labeled processes could be seen in the LOT at higher magnification (Fig. 2*A Inset*). The contralateral anterior olfactory nucleus (AON) contained labeled cells (Fig. 2*B*). Other than the AON, no labeling was seen in the contralateral OB. These results suggest that most of the pyramidal cell labeling arose from third-order infection through granule cell synapses because if second-order pyramidal cells were present in the AON, then mitral and tufted cells in the contralateral OB would receive virus in the third-order infection stage.

Within the ipsilateral OB (Fig. 2*C*) the majority of the fluorescent cells were restricted to the injection (lateral) side of the ipsilateral OB. The distribution of labeled cell populations in the medial quadrant showed similar columns in the GCL as in the lateral side, but with reduced frequency. There were tufted cells (Fig. 2*C*, arrow) and granule cells labeled in the opposite side, but few mitral cells. The same-side specificity was apparent after anterior dorsomedial injections as well (data not shown). There was significant staining of cells in the dorsal and ventral areas with injections into both of these sides.

To confirm that the medial-lateral specificity was not exclusive to the dorsoanterior area of the bulb, we next performed injections into the anterior ventrolateral (Fig. 2*D Left*) and anterior ventromedial (Fig. 2*D Right*) areas of the OB. The injections shown in Fig. 2*D* were performed in the same animal. The general patterning and medial-lateral specificity were consistent for all bulb injections. Four posterior sites within the OB corresponding to the previous four anterior injections were made as well, yielding staining similar to the anterior injections (data not shown).

A striking feature common to the staining patterns with all OB injections was that granule cell populations were labeled in a distributed, radial pattern. Closer inspection showed that three cell populations contributed to this radial pattern, as shown in more detail in Fig. 3. In some areas, there were labeled mitral and tufted cells associated with the labeled granule cells (Fig. 3*A*). In other areas, there were labeled mitral and tufted cells not associated with staining in the nearby GCL (Fig. 3*A*). There were also groups of labeled granule cells not associated with labeled mitral or tufted cells (Fig. 3*B*).

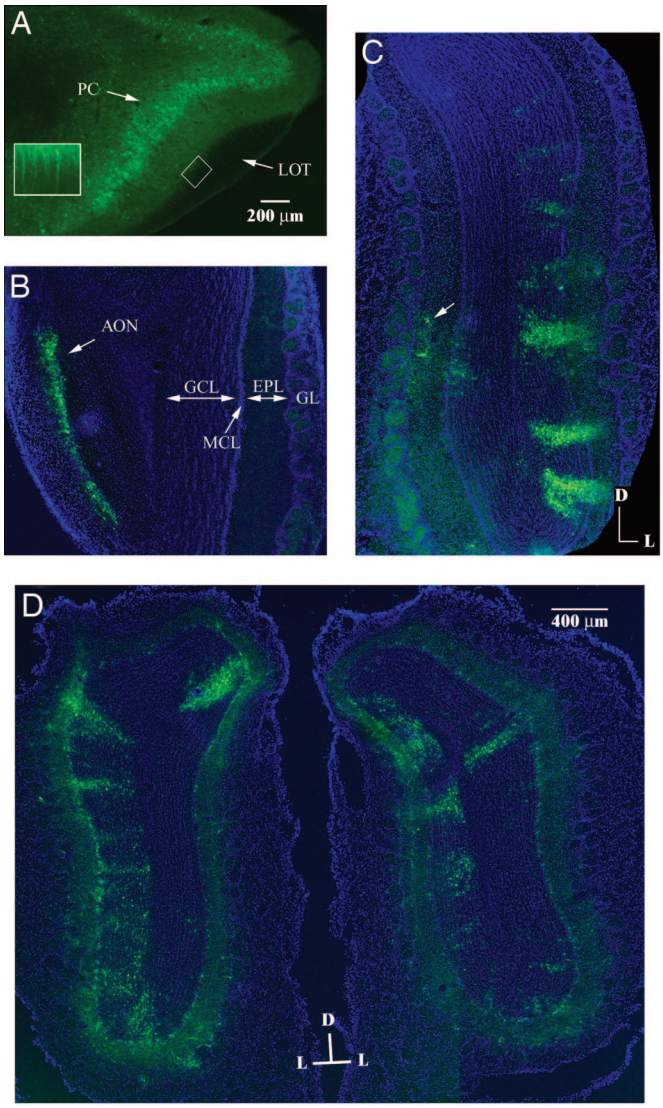


**Fig. 2.** PRV staining patterns after OB injections. A-C) Coronal sections of the rat brain 3 days after PRV injection into the anterior dorsolateral OB at ×40 magnification. Virus-infected cells are stained green (GFP and α-GFP), and all cell nuclei in *B* and *C* are blue (DAPI). Scale bar in *A* applies to *A–C*. (*A*) The ipsilateral piriform cortex (PC) is prominently labeled in this section ≈3.7 mm anterior to Bregma, whereas the LOT is not. Note, however, several processes penetrating the LOT (*Inset*, ×200 magnification of boxed region). (*B*) A section showing the contralateral bulb ≈6.5 mm anterior to Bregma. Only the anterior olfactory nucleus (AON) contains PRV. MCL, mitral cell layer; EPL, external plexiform layer; GL, glomerular layer. (*C*) A section of the ipsilateral bulb posterior to the injection site. The majority of PRV-stained cells appear in the injection-side half of the OB in radial patterns. The arrow shows a labeled tufted cell in the medial side, possibly an intrabulbar projection neuron identified by Belluscio *et al.* (50). (*D*) Coronal section of the rat OB 3 days after PRV injections into the anterior ventrolateral (*Left*) and anterior ventromedial (*Right*) OBs of the same animal (overlay of two fields at ×40 magnification). As with the anterior dorsal injections, the majority of columns appear in the ipsilateral half of the OB.

NEUROSCIENCE

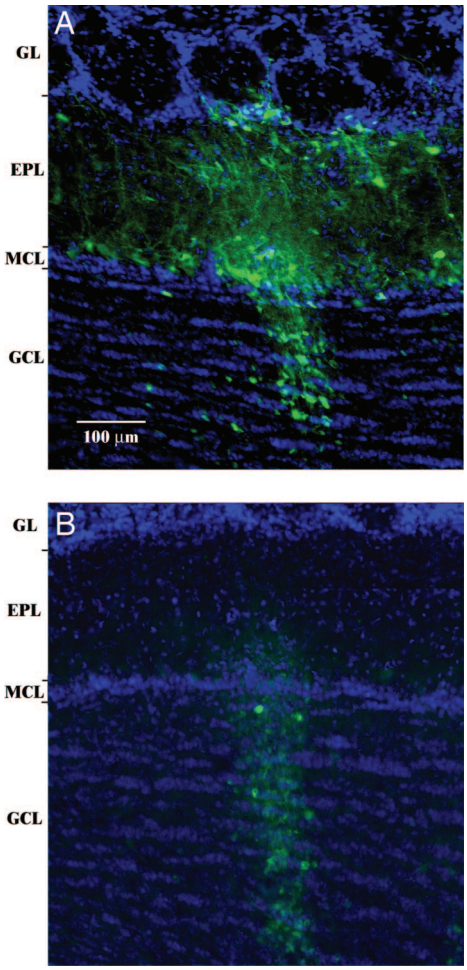


**Fig. 3.** Columns with and without associated mitral/tufted cells. Coronal sections of the rat OB 3 days after PRV injection into the dorsomedial OB (two fields overlain, colored as in Fig. 2). (*A*) A column with associated mitral and tufted cells. Mitral and tufted cells are labeled without granule cell columns to both sides of the full column. (*B*) A granule cell-only column with no mitral or tufted cells stained.

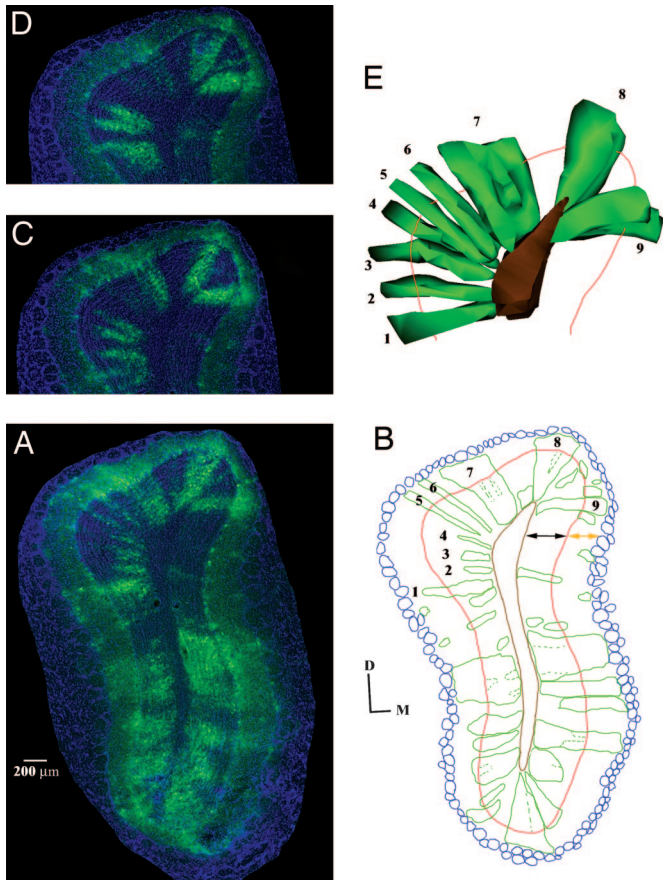


**Fig. 4.** OB columns from anterior piriform cortex PRV injection. (*A*) Coronal section of the rat OB 3 days after injection of PRV into the anterior piriform cortex, colored as in Fig. 2. (*B*) Schematic of the OB organization of *A*. Blue, glomeruli; red, mitral cell layer (MCL); brown, subventricular zone; green, virus-labeled columns. Black arrows indicate the GCL; orange arrows the external plexiform layer. Dashed green lines indicate areas that may be interpreted as further division of a larger column. Columns 5 and 6 extend from the glomerular layer to the deepest area of the GCL nearly completely within the confines of the 60-$\mu$m section shown. Columns 1–4 also extend from the deep GCL to single glomeruli residing in other sections. (*C* and *D*) Adjacent sections anterior to *A*, showing the progression of columns 2–4. (*E*) A 3D reconstruction of the selected columns through 11 sections, 5 anterior and 5 posterior to *A*. The red line represents the MCL in *A* for reference.

**Radial Patterns in the OB from Piriform Cortex.** To rule out the unlikely possibility that local damage or bloodstream transmission within the OB could account for the radial patterns, we injected a distal site, anterior piriform cortex, that is two retrograde synapses from the granule cells in the OB: from the pyramidal cell dendrite to the mitral cell axon terminal, retrogradely transported to the mitral cell bodies and dendrites, and from there to the granule cells. Based on previous studies, we predicted that only a subset of the total glomerular unit input would be represented in a given cortical region (31–35).

In a representative experiment, PRV was injected into the rat anterior piriform cortex. The injection site diameter was ≈500 $\mu$m, covering all cortical layers (Fig. 7 *B* and *C*). Sections were prepared as described earlier. In all of these experiments ($n$ = 10), radial patterns of labeled cells were seen within the ipsilateral OB. In the example of Fig. 4*A*, radial patterns were seen throughout the circumference of the bulb. The labeling was particularly evident in the GCL. As shown, in a single histological section, the patterns had varying widths and varying cross-laminar extensions, often reaching from the glomerulus through the external plexiform layer (EPL) to the deepest part of the GCL next to the subventricular zone (SVZ) (Fig. 4*A*). These variations are shown more clearly in the outlines in Fig. 4*B*.

These results provided strong support for the radial arrangements of cells within the OB and ruled out local spread from OB injections as a possible mechanism for these arrangements. We carried out detailed analysis of these radial populations by using data from cortical injections. In single sections, populations of granule, mitral, and tufted cells could be seen making up radial arrangements (see Fig. 4*B*, numbers 5 and 6) that extended partially through the layers; we used serial sections to determine the extent to which the full populations extended across all layers from the SVZ to the glomerulus (e.g., Fig. 4*B*, numbers 2–4).

Observations of adjacent sections suggested that limited labeled populations (Fig. 4 *C* and *D*, numbers 2–4) actually extend across the laminae. A stack of serial sections of the OB therefore was assembled in register as the basis for building a 3D reconstruction of a representative region. Fig. 4*E* shows the regions numbered from Fig. 4 *A* and *B* reconstructed in their entirety. Five sections anterior and five sections posterior to the section in Fig. 4*A* contained the associated labeled cells. Narrow populations 1–6 each project from a single glomerulus, whereas wider areas 7–9 project from multiple glomeruli. In our recon-

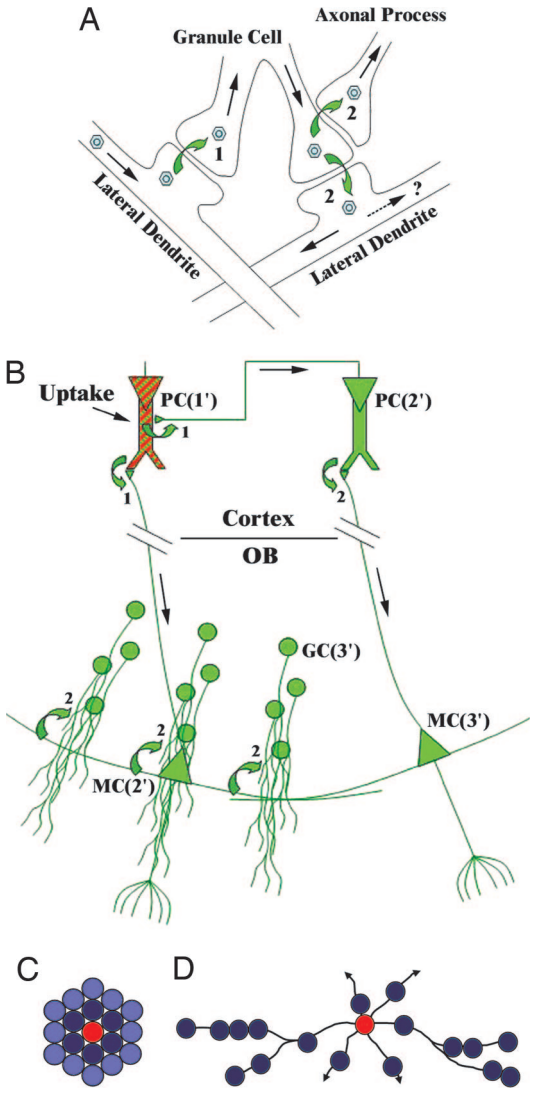


**Fig. 5.** Models for PRV transfer and staining patterns in the OB. (*A*) A diagram of the retrograde synaptic transfer of PRV (hexagrams) in OB neurons. Virus comes from the soma of a first-order infected mitral cell to the left and travels down the lateral dendrite to a granule cell, crossing the first synapse (1 in diagram). Virus then replicates within the granule cell and passes to axonal processes, including mitral cell axon collaterals and centrifugal fibers (2 at top). Because of the reciprocal nature of the GC synapse, virus also may pass to another secondary dendrite (2 at bottom), although it is not known whether productive infection can occur through this transmission route. (*B*) A diagram showing an interpretation of the viral-staining patterns from piriform cortex injection. The virus is taken up at the injection site by pyramidal cells (PC) in the cortex (red and green cell, top left; 1′, 2′ and 3′ refer to first-, second-, and third-order neurons, respectively). After 24 h, the virus replicates and crosses the synapses to axons from the cortical cells dendrites (1 in diagram). The virus travels in a retrograde manner to other pyramidal cells in the cortex through the cortico-cortical connections and to mitral cells (MC) in the OB through the lateral olfactory tract (tufted and periglomerular cells are omitted for simplification). Twenty-four hours later, virus is visible by GFP fluorescence in the second-order neurons, and the second synapses are crossed (2 in diagram). Another 24 h shows fluorescence in the granule cells (GC) that represent third-order neurons (*Left*) and lone mitral cells that are also third order neurons infection from second order pyramidal cells (*Right*). Note that the rightmost granule cell population is labeled from infection by the lateral dendrite from the second-order mitral cell on the left, not the third order mitral cell on the right. (*C* and *D*) Distance-dependent center-surround vs. selective inhibition. Circles represent a top view of glomerular units. (*C*) In a distance-dependent center-surround inhibition model, the activated glomerulus (red) inhibits surrounding glomeruli in a distance-dependent manner. Inhibition is shown by the intensity of blue. (*D*) In a selective inhibition model, the activated glomerulus inhibits selectively connected glomeruli through the synapses on the mitral and tufted cell secondary dendrites at the granule cell level. Such connections would extend in all directions from the activated glomerulus (arrows). This model is consistent with a recent computational models of odor coding (36, 51).

structions, 95% of the radial patterns of labeling extended across all layers, from the SVZ to the glomerular layer (GL). When they do not extend across all layers, such as with the GCL-only columns, the column still extends the full length of the GCL from the SVZ to the mitral cell layer (MCL).

These analyses suggest that radially organized populations of neurons in the OB form organizational units that are anatomically columnar in nature.

**Columns Are Associated with a Single Glomerulus.** We next wished to establish the relation of the columns to the most prominent anatomical feature of the OB: the glomeruli. We first identified the narrowest columns that, from the 3D reconstructions, extended to the glomerular layer. All of the columns we examined were found to be centered on a single glomerulus, suggesting that a complete single-radial column was anatomically related to a single olfactory glomerulus. This finding with anterior piriform cortex injections was entirely consistent with the observations of individual narrow columns centered on individual glomeruli that can be seen with OB injections. The larger column units likely represent aggregations of multiple, and possibly related, single glomerular units (see *Supporting Text* and Figs. 8–10, which are published as supporting information on the PNAS web site). The varying degrees of labeling in the GCL are thought to be related directly to the number of mitral or tufted cells labeled as second-order neurons for a given column.

## Discussion

**PRV Is Transported Across Reciprocal Dendrodendritic Synapses.** In this study, we used PRV to probe the synaptic organization of the olfactory system through intracranial injection. Despite the unusual synaptic arrangements in the OB, in which dendrites are presynaptic to other dendrites, it is possible to specify explicitly the pathway taken by the virus in creating the patterns that have been observed (Fig. 5). For consistency, we will refer to the neurons first receiving virus at the injection site as first-order neurons, the neurons one synapse from first-order neurons as second-order neurons, and those two synapses from the injection site as third-order neurons.

**OB Injections.** For OB injections (Fig. 5*A*), the sequence of uptake and transport can be inferred from previous studies in other systems (26–29). From these systems, it is known that after initial uptake into neurons, the virus is transported through the cell to be transferred across synapses on the dendrites in a retrograde manner. In the case of mitral and tufted cells, which are both pre- and postsynaptic to granule cell processes, viral transfer would imply transport retrogradely at the inhibitory granule-to-mitral synapses on the soma and secondary dendrites (Fig. 5*A*, see no. 1). The profuse labeling of granule cells in the vicinity of the injection site indicates that the virus has followed this course. From the granule cell dendrites, there would be further transport into the terminals of mitral and tufted cell axon collaterals (if present) and the terminals of axons from centrifugal fibers, e.g., pyramidal cells in the olfactory cortex (Fig. 5*A*, see no. 2). Further transport in the long lateral dendrites of mitral and tufted cells also is expected (Fig. 5*A*, dotted line).

**Piriform Cortex Injections.** Circuit tracing from anterior piriform cortex injection resulted in a subset of labeled neurons in the OB, as opposed to diffuse labeling, consistent with the predictions of

previous work (31, 32, 34, 35). For anterior piriform cortex injections (Fig. 5*B*), it appears that there is local uptake into pyramidal cells in and around the injection site, followed by transport through the pyramidal cell dendrites and retrograde transfer to the terminals of mitral and tufted cell axons arriving from the LOT. There is also transfer to the terminals of axon collaterals of neighboring cortical pyramidal cells (see Fig. 5 diagram). Pyramidal-to-pyramidal cell transfer is followed by retrograde virus transport in the axons of mitral and tufted cells to their cell bodies in the OB and out into their lateral and primary dendrites. The lateral dendrites are then the source for further virus transfer retrogradely to infect granule cells.

**Circuit Tracing Reveals a Narrow Glomerular Unit Column.** It is generally accepted that the glomerular unit constitutes an information-processing module (7). This module has been hypothesized to extend into the GVL but with a more diffuse distribution (37, 38). Our results suggest that the minimal granule cell columns are an extension from the glomerular unit of mitral and tufted cells. With the available data, it is not possible to comment in detail on the interconnections between cells within the focal units that are detected after viral tracer injection. One of the hypothesized features of a column is the higher degree of connectivity between cells within the column. Although high connectivity is possible in the units described in the bulb, the data presented here does not allow a great degree of resolution of the local connectivity within each unit. Therefore, further study on the neurons identified by synaptic connectivity to be grouped in cylindrical modules will be necessary to compare and contrast the OB modules with columns found in other systems.

A surprising finding of this study is the integrity of the diameter of the columns through the full GCL. The dendritic arbors of OB granule cells can extend 3–5 glomeruli (39). The broad dendritic organization may lead one to speculate that the minimal column would also be 3–5 glomeruli wide, but the results presented here show that there is a synaptic pathway that reveals a more narrowly defined column. This finding suggests that single-granule cells whose arbors extend across three glomeruli may not necessarily form synapses with mitral or tufted cells from all of these glomeruli. Our results imply that one possible function of the GC dendritic spread is to allow for contact with a wider representation of mitral and tufted cell secondary dendrites. This hypothesized arrangement would allow each glomerulus to exchange information with a large number of distal glomeruli.

Previous studies of olfactory modules by using measures that did not identify synaptic connectivity showed more diffuse patterns in the GCL. These studies contributed significantly to the understanding of modular organization in the OB. Kauer and Cinelli (38) found comparatively diffuse activation within the GCL after odorant stimulation as measured by 2-deoxyglucose turnover, an indirect measure of neuronal activity levels. The same study found similar results by using voltage sensitive dyes, although this method was applied only to salamander. The differences could be due to either gap junctions that the virus does not cross or centrifugal input excitation that would require anterograde tracer to identify. This is also a possible explanation of why Guthrie *et al.* (37) observed flask-shaped, rather than columnar-staining, patterns in the GCL based on c-fos mRNA levels, another indirect measure of high activity. Although the dimensions shown by these other studies are larger and less well defined than those revealed by PRV, we interpret that each of these measures reflect different aspects of the modular unit organization.

**Circuit Tracing Shows Selective Patterning of Granule Cell Connections on Lateral Dendrites.** The distributed radial patterning of olfactory columns was not confined to restricted areas of the OB after either local injection into the OB or the anterior piriform cortex but was interspersed in many areas. We observed some columns with only granule cells stained, as the one shown in Fig. 3*B* in detail. One possibility is that the clustering in these columns originates from patches of granule cell connections interspersed along the whole length of the mitral and tufted cell lateral dendrites. This explanation assumes that interspersed areas of lateral dendrites do not contain granule cell connections. Our interpretation is not inconsistent with electron microscopy results, although the distances involved in our proposed model are not accessible by using this technique (40).

An alternative hypothesis is that the virus may be selectively passing through only the most active of the synapses. There is no evidence to date for or against activity dependence in the case of PRV infection of the olfactory system. However, if PRV transmission relies on active synapses (as we suspect), the finding of robust columnar structure within the GCL by using PRV implies that the column is a functional, activity-dependent unit.

The distinct patterning suggests that selectively distributed inhibition occurs at the GCL. In the on-center, off-surround inhibition network of the retina, the strength of inhibition is a graded function of distance (Fig. 5*C*; ref. 41). By contrast, the granule cell inhibitory action excited by mitral and tufted cell lateral dendrites appears to be highly selective, not restricted to neighbor relationships (Fig. 5*D*). This organization implies that mitral and tufted cells can collect information from specific glomeruli at varying distances and that the center-surround model may need to be revisited for the OB (42). It has been shown that action potentials can faithfully propagate up to 1,000 $\mu$m along mitral cell lateral dendrites and, therefore, activate granule cells at distances relevant to our model (43, 44). This connectivity observed in the adult may be the result of experience-dependent changes due to coincident firing of projection neurons (and therefore granule cells) from distant glomeruli. The interglomerular network also may possess mechanisms for selective inhibition, because Aungst *et al.* (14) showed that short-axon cells can extend processes 20–30 glomeruli distant. One may hypothesize that the selective lateral connectivity reflects (or is responsible for) the response domains identified by multiple methods (45–48).

## Materials and Methods

All of the animal use procedures in this study conformed to the Guide for the Care and Use of Laboratory Animals (1996, National Academy of Sciences) and were approved by the Yale Institutional Animal Care and Use Committee.

An attenuated PRV strain (Bartha), which was further modified to express EGFP (or mRed1) under control of the cytomegalovirus immediate early promoter, PRV-152 (or PRV-614), was used for transneuronal tracing of synaptic pathways in this study, a gift from Lynn W. Enquist (Princeton University, Princeton, NJ). PRV passes transsynaptically in a retrograde manner from axon terminals to the cell nucleus, where replication occurs. Fluorescence therefore indicates transfer of virus to the nucleus and adequate expression of fluorescent protein.

Thirty-four Sprague–Dawley rats age 4–6 weeks were used in this study. All experiments were performed at least in triplicate. Detailed published protocols in ref. 49 were followed for viral injections. Rats were anesthetized with 75 mg/kg ketamine and 5 mg/kg xylazine by i.p. injection, and additional drug was added as necessary. After anesthetization, 100 nl of PRV [adjusted with PBS to $1 \times 10^8$ pfu/ml with 1 $\mu$m diameter green or blue fluorescent microspheres (1:10 stock solution, Molecular Probes, Eugene, OR) added in a 1:20 volume ratio to mark the site] was injected by using a Hamilton syringe (Fisher Scientific, Pitts-

burgh, PA) with a 33-gauge needle into the indicated areas by using a stereotaxic instrument (Stoelting, Wood Dale, IL). The rate of injection was 20 nl/min, controlled by a Nano-Injector system (Stoelting; this instrument was found to be vital for reproducible injection volumes). After 15 min to allow diffusion of the bolus, the syringe was removed slowly.

Three days after injection (70–74 h), the animals were deeply anesthetized by using urethane then perfused transcardially with 120 ml of PBS followed by 60 ml of a 4% paraformaldehyde (PFA) solution in PBS. The brain was extracted after fixation and postfixed in PFA overnight. Before sectioning, the fixed brains were cryoprotected in fixative solution with 25% sucrose.

The brains were embedded in frozen OCT medium (Tissue-Tek; Fisher Scientific) for sectioning on a Reichert-Jung 2800 Frigocut E cryostat (Leica, Bannockbum, IL). Coronal sections were prepared at thicknesses of 40–60 mm. The slides (Superfrost Plus; Fisher Scientific) with tissue sections requiring signal amplification were incubated in a 1 mg/ml anti-GFP antibody solution (Rockland Immunochemicals, Gilbertsville, PA) with 5% milk and 0.2% Triton X-100 in PBS at 4°C overnight. The tissue sections were treated further by washing with PBS twice and then incubated for 10 min in a solution of 2.5% Sudan black in 70% MeOH to minimize autofluorescence, followed by 5-min incubation in 70% ethanol. For cellular nuclei staining, the tissue sections were mounted in Vecta-Shield mounting medium containing DAPI (Vector Laboratories, Burlingame, CA). Sections were examined by using an Olympus (Melville, NY) BHX2 microscope equipped with an Olympus Magnafire digital camera. Injections also were performed in the absence of injection site indicator beads and showed staining patterns indistinguishable from those with a bead, demonstrating that the bead did not play a role in the viral-staining patterns.

Images were colored, manipulated for brightness and contrast, and cropped by using Adobe Photoshop 6.0.1 (San Jose, CA). Sections were aligned, and 3D reconstructions and distance measurements were performed by using Reconstruct 1.0.4.2 (courtesy of Kristen Harris and John Fiala, Boston University, Boston, MA; free download from www.synapses.bu.edu). Distance measures were not adjusted for shrinkage of samples due to tissue processing. Diagram figures were created by using Microsoft PowerPoint 2002 (Redmond, WA), and bar graphs were created by using Microsoft Excel 2002, and further manipulated in Adobe Photoshop.

We thank Drs. L. W. Enquist for providing the PRV strains and advice concerning their use, and M. Luo for technical advice and helpful discussions. This work was supported by National Institutes of Health Grants DC003918 (to W.R.C.) and DC00086 (to G.M.S.).

1. Lorente de No, R. (1938) in *Physiology of the Nervous System*, ed. Fulton, J. F. (Oxford Univ. Press, London), pp. 291–339.
2. Mountcastle, V. B. (1957) *J. Neurophysiol.* **20,** 408–434.
3. Hubel, D. H. & Wiesel, T. N. (1968) *J. Physiol.* **195,** 215–243.
4. Hubel, D. H. & Wiesel, T. N. (1962) *J. Physiol.* **160,** 106–154.
5. Imig, T. J. & Adrian, H. O. (1977) *Brain Res.* **138,** 241–257.
6. Goldman, P. S. & Nauta, W. J. (1977) *Brain Res.* **122,** 393–413.
7. Shepherd, G. M., Chen, W. R. & Greer, C. A. (2004) in *The Synaptic Organization of the Brain*, ed. Shepherd, G. M. (Oxford Univ. Press, New York), pp. 165–216.
8. Ressler, K. J., Sullivan, S. L. & Buck, L. B. (1993) *Cell* **73,** 597–609.
9. Vassar, R., Ngai, J. & Axel, R. (1993) *Cell* **74,** 309–318.
10. Clancy, A. N., Schoenfeld, T. A., Forbes, W. B. & Macrides, F. (1994) *Brain Res. Bull.* **34,** 211–241.
11. Schoenfeld, T. A., Clancy, A. N., Forbes, W. B. & Macrides, F. (1994) *Brain Res. Bull.* **34,** 183–210.
12. Mombaerts, P., Wang, F., Dulac, C., Chao, S. K., Nemes, A., Mendelsohn, M., Edmondson, J. & Axel, R. (1996) *Cell* **87,** 675–686.
13. Treloar, H. B., Feinstein, P., Mombaerts, P. & Greer, C. A. (2002) *J. Neurosci.* **22,** 2469–2477.
14. Aungst, J. L., Heyward, P. M., Puche, A. C., Karnup, S. V., Hayar, A., Szabo, G. & Shipley, M. T. (2003) *Nature* **426,** 623–629.
15. Rall, W., Shepherd, G. M., Reese, T. S. & Brightman, M. W. (1966) *Exp. Neurol.* **14,** 44–56.
16. Price, J. L. & Powell, T. P. (1970) *J. Cell Sci.* **7,** 125–155.
17. Pinching, A. J. & Powell, T. P. (1971) *J. Cell Sci.* **9,** 305–345.
18. Pinching, A. J. & Powell, T. P. (1971) *J. Cell Sci.* **9,** 379–409.
19. Rall, W. & Shepherd, G. M. (1968) *J. Neurophysiol.* **31,** 884–915.
20. Mori, K., Kishi, K. & Ojima, H. (1983) *J. Comp. Neurol.* **219,** 339–355.
21. Yokoi, M., Mori, K. & Nakanishi, S. (1995) *Proc. Natl. Acad. Sci. USA* **92,** 3371–3375.
22. Mori, K., Nagao, H. & Yoshihara, Y. (1999) *Science* **286,** 711–715.
23. Price, J. L. & Powell, T. P. (1970) *J. Anat.* **107,** 215–237.
24. Pinching, A. J. & Powell, T. P. (1972) *J. Cell Sci.* **10,** 621–635.
25. Enquist, L. W. (2002) *J. Infect. Dis.* **186,** Suppl. 2, S209–S214.
26. Standish, A., Enquist, L. W., Miselis, R. R. & Schwaber, J. S. (1995) *J. Neurovirol.* **1,** 359–368.
27. Billig, I., Foris, J. M., Card, J. P. & Yates, B. J. (1999) *Brain Res.* **820,** 31–44.
28. Billig, I., Foris, J. M., Enquist, L. W., Card, J. P. & Yates, B. J. (2000) *J. Neurosci.* **20,** 7446–7454.
29. Smith, B. N., Banfield, B. W., Smeraski, C. A., Wilcox, C. L., Dudek, F. E., Enquist, L. W. & Pickard, G. E. (2000) *Proc. Natl. Acad. Sci. USA* **97,** 9264–9269.
30. Banfield, B. W., Kaufman, J. D., Randall, J. A. & Pickard, G. E. (2003) *J. Virol.* **77,** 10106–10112.
31. Haberly, L. B. & Price, J. L. (1977) *Brain Res.* **129,** 152–157.
32. Luskin, M. B. & Price, J. L. (1982) *J. Comp. Neurol.* **209,** 249–263.
33. Buonviso, N., Revial, M. F. & Jourdan, F. (1991) *Eur. J. Neurosci.* **3,** 493–500.
34. Zou, Z., Horowitz, L. F., Montmayeur, J. P., Snapper, S. & Buck, L. B. (2001) *Nature* **414,** 173–179.
35. Zou, Z., Li, F. & Buck, L. B. (2005) *Proc. Natl. Acad. Sci. USA* **102,** 7724–7729.
36. Linster, C., Sachse, S. & Galizia, C. G. (2005) *J. Neurophysiol.* **93,** 3410–3417.
37. Guthrie, K. M., Anderson, A. J., Leon, M. & Gall, C. (1993) *Proc. Natl. Acad. Sci. USA* **90,** 3329–3333.
38. Kauer, J. S. & Cinelli, A. R. (1993) *Microsc. Res. Tech.* **24,** 157–167.
39. Price, J. L. & Powell, T. P. (1970) *J. Cell Sci.* **7,** 91–123.
40. Woolf, T. B., Shepherd, G. M. & Greer, C. A. (1991) *Synapse* **7,** 181–192.
41. Sterling, P. & Demb, J. B. (2004) *Retina* (Oxford Univ. Press, New York).
42. Laurent, G. (1999) *Science* **286,** 723–728.
43. Xiong, W. & Chen, W. R. (2002) *Neuron* **34,** 115–126.
44. Lowe, G. (2002) *J. Neurophysiol.* **88,** 64–85.
45. Leon, M. & Johnson, B. A. (2003) *Brain Res. Rev.* **42,** 23–32.
46. Xu, F., Greer, C. A. & Shepherd, G. M. (2000) *J. Comp. Neurol.* **422,** 489–495.
47. Mori, K., Takahashi, Y. K., Igarashi, K. M. & Yamaguchi, M. (2006) *Physiol. Rev.* **86,** 409–433.
48. Schaefer, M. L., Finger, T. E. & Restrepo, D. (2001) *J. Comp. Neurol.* **436,** 351–362.
49. Card, J. P. & Enquist, L. W. (1999) in *Current Protocols in Neuroscience*, ed. Crawley, J. N. (Wiley, New York), pp. 1.5.1–1.5.28.
50. Belluscio, L., Lodovichi, C., Feinstein, P., Mombaerts, P. & Katz, L. C. (2002) *Nature* **419,** 296–300.
51. Cleland, T. A. & Sethupathy, P. (2006) *BMC Neurosci.* **7,** 7.